Determining Gas-Phase Chelation of Zinc, Cadmium, and Copper Cations With HisHis Dipeptide using Action Spectroscopy and Theoretical Calculations

Brandon C. Stevenson,<sup>†</sup> Giel Berden,<sup>‡</sup> Jonathan Martens,<sup>‡</sup> Jos Oomens,<sup>‡,§</sup> and P. B. Armentrout<sup>†,\*</sup>

†Department of Chemistry, University of Utah, 315 South 1400 East, Room 2020, Salt Lake City,
Utah 84112, USA

<sup>‡</sup>Radboud University, Institute for Molecules and Materials, FELIX Laboratory, Toernooiveld 7, 6525 ED Nijmegen, The Netherlands

§van't Hoff Institute for Molecular Sciences, University of Amsterdam, Science Park 904, NL-1098 XH Amsterdam, The Netherlands

\* Corresponding author, e-mail: armentrout@chem.utah.edu

#### **Abstract**

Using light generated by an infrared free electron laser, action spectroscopy was performed on doubly charged complexes of the metalated dipeptide histidyl-histidine (HisHis). Metal cations used were zinc, cadmium, and copper. Molecular dynamics and quantum-chemical calculations were used to screen a large number of conformers, whose theoretical infrared spectra were compared to the recorded action spectra of these metalated complexes. The zinc and cadmium spectra display dominant features associated with an iminol binding motif of the HisHis ligand, where the metal ion coordinates with both *pros* ( $\pi$ ) nitrogens of the imidazole sidechains, the terminal carbonyl oxygen, and the backbone nitrogen for which the hydrogen ordinarily bound here has migrated to a carbonyl. The copper complex was difficult to assign to a single species, because a few predicted bands are absent from the experimental spectrum. The theoretical single point energies were also calculated for all structures examined, and DFT methods were found to describe the ion conformer populations in the case of the zinc and cadmium chelates better than the MP2 prediction.

### Introduction

Transition metals and their role in biological systems are a main driver in the regulation and progression of disease and proper homeostatic function. A significant step in the pathogenesis of Alzheimer's disease is the aggregation of histidine (His) rich amyloid- $\beta$  (A $\beta$ )peptides.[1] This aggregation is facilitated by zinc ions that cross-link peptides by forming intermolecular His—Zn<sup>2+</sup>—His linkages where the zinc ion coordinates with the *tele* ( $\tau$ ) nitrogen of the imidazole ring.[2-4] The introduction of copper has been shown to inhibit the Zn(II) induced A $\beta$  aggregates by preferentially forming His—Cu<sup>2+</sup> chelates, where the Cu(II) ion coordinates with the *pros* ( $\pi$ ) nitrogen of the imidazole sidechain or the amine nitrogen.[5]

Zinc finger proteins, one of the most abundant groups of proteins, are so-named for the zinc ion that maintains the zinc finger structure by coordinating with cysteine and histidine residues. The classical zinc finger coordinates the Zn(II) ion with two cysteine residues from one chain and two histidine residues from another, enhancing the conformational stability of the domain.[6] Zinc finger proteins have been found to play a critical part in effective protein folding, gene expression, cellular signaling, and tumor suppression.[7] Cadmium can replace the zinc metal center, disrupting the metal site's activity. The metal modulation of DNA binding activity of zinc finger proteins has been widely studied.[8-14] This disruption is notable in that the DNA binding of the zinc finger protein is not deactivated, as one would expect if the cadmium metal induced a significant conformational change.

Elucidating the fundamental interactions of the zinc, cadmium, and copper ions and the coordinating amino acid residues is critical in understanding disease progression and the role of these metals in human health. To examine these basic interactions without the complicating effects of solvent or tertiary structural effects, we have elected to study the biomimetic complexes of  $M^{2+}(HisHis)$  (where M = Zn, Cd, and Cu) using infrared multiple photon dissociation (IRMPD) action spectroscopy and quantum-chemical calculations. Comparison between IRMPD and simulated spectra permits determination of the dominant conformation of the chelates formed in

the vacuum of the mass spectrometer.[15-17]

## **Experimental and Computational Section**

Mass Spectrometry and IRMPD Photodissociation

Light from the FELIX beamline at the Free-Electron Laser for Infrared eXperiments (FELIX) Laboratory at Radboud University, the Netherlands, was used to irradiate the massisolated biomimetic complexes of M<sup>2+</sup>(HisHis) in the 600-1900 cm<sup>-1</sup> fingerprint region.[18] IRMPD spectra were obtained using a quadrupole ion trap (QIT) mass spectrometer (Bruker, Amazon Speed ETD) modified for optical access to the ion trap.[19] To generate the species of interest, solutions of metal chloride and HisHis dipeptide were mixed in equimolar amounts and diluted in methanol, resulting in concentrations of roughly 10<sup>-6</sup> M. All reagents were obtained from commercial sources and used without any further purification. The desired ions were then generated using an electrospray ionization source.

Plotting the photofragmentation yield (Y) as a function of the laser wavenumber provides a surrogate IR spectrum of the trapped ions that can be compared with simulated spectra. Specifically, the yield was calculated using the equation  $Y = -\ln[\sum I_P / (\sum I_F + \sum I_P)]$ , where the precursor ( $I_P$ ) and fragment ( $I_F$ ) ion mass components are the integrated intensities.[20] All experimental spectra were power-corrected to account for any wavelength-dependent variations in laser power.[20, 21]

## Computational Details

A previously detailed simulated annealing protocol generated Zn<sup>2+</sup> and Cu<sup>2+</sup> starting structures.[22-26] Unique low-energy structures underwent subsequent geometry optimizations with the B3LYP/6-311+G(d,p) method using the Gaussian16 suite of programs.[27] To generate Cd<sup>2+</sup> conformers, the metal ion in the Zn<sup>2+</sup> and Cu<sup>2+</sup> structures was replaced with a Cd<sup>2+</sup> ion. These Cd<sup>2+</sup> geometries were geometry optimized at the B3LYP/def2-TZVP level of theory, where the basis set included a 28-electron effective core potential (ECP) on Cd obtained from the Basis Set Exchange.[28] For all three metalated species, the optimized structures were used to calculate

vibrational frequencies using the same method as the geometry optimization. Optimized geometries were used to calculate single-point energies (SPE) at the B3LYP, B3P86, and MP2 levels of theory using larger basis sets (Zn<sup>2+</sup> and Cu<sup>2+</sup>, 6-311+G(2d,2p); Cd<sup>2+</sup> def2-TZVPP). To test the effect of dispersion forces on these complexes, geometries and frequencies were reoptimized using the B3LYP-GD3BJ empirical dispersion method again using the 6-311+G(d,p) or def2-TZVP basis sets.[29, 30] The larger basis sets (Zn<sup>2+</sup>, 6-311+G(2d,2p); Cd<sup>2+</sup>, def2-TZVPP) were also used to calculate B3LYP-GD3BJ SPEs.

For the analysis of relative energies, theoretical frequencies were scaled by 0.9896 to obtain 0 K relative enthalpies and 298 K Gibbs energies.[31] For comparison to the experimental IR spectra, vibrational frequencies were scaled by 0.975 and broadened using a Gaussian line shape (25 cm<sup>-1</sup> FWHM).[32] Different scaling factors for the energies and vibrational frequencies were used in order to account for anharmonic shifts in the simulated spectra. This combination of theoretical methods and scaling factors have been used satisfactorily elsewhere on similar systems.[33-51]

### **Results and Discussion**

Relative Energies and Structures of Zn Complexes

## Nomenclature

To ease direct comparison of the explored  $M^{2+}(HisHis)$  structures, the naming system shown in Figure 1 will be used. The metal binding sites for each conformation, listed from N to C terminus, are given in square brackets. N is for the amine nitrogen,  $N^{1s}$  is for the  $\pi$  (pros) nitrogen of the first histidine residue,  $CO^B$  is for the backbone carbonyl oxygen,  $N^B$  is for the backbone nitrogen where the hydrogen has migrated (typically to a carbonyl oxygen),  $N^{2s}$  is for the  $\pi$  nitrogen of the second histidine residue, and CO is for the carboxylic acid oxygen. In the case where two structures share the same metal binding sites, the contents of the square brackets are followed by a number in parentheses, where the structures are numbered in order of their relative energies (from lowest- to higher-energy, ordered according to their average relative 298 K Gibbs energies).

Structures and relative energies for the  $Zn^{2+}$  (HisHis) complexes are detailed in Table 1 and Figure 2. For the discussion of relative energies, the Gibbs energies at 298 K will be used as these energies have been found to reasonably describe the ion population temperature in previous experiments.[33-51] The B3LYP, B3P86, and B3LYP-GD3BJ levels of theory all predict the  $[N^{1s},N^B,N^{2s},CO](1)$  structure to be the ground structure (GS). This structure is characterized by the divalent  $Zn^{2+}$  coordinating with both  $\pi$  nitrogens of the imidazole sidechains, the C-terminal carbonyl oxygen, and the backbone nitrogen. The backbone nitrogen is available for this coordination as the hydrogen ordinarily bound to this atom has migrated to a nearby nucleophile (here, the backbone amide O atom). This results in an iminol structure, first detailed by Dunbar and coworkers, where the backbone nitrogen is a strong Lewis base that is stabilized by coordination with the metal ion.[52] A hydrogen bond between the terminal amine and the newly hydrogenated backbone CO further stabilizes the peptide backbone.

Three  $[N,N^{1s},N^B,N^{2s}]$  structures were located above the DFT GS, where the Zn metal ion coordinates with the amino nitrogen, both  $\pi$  nitrogens of the imidazole sidechains, and the backbone nitrogen. Subtle differences in the hydrogen bonding along the peptide bonding differentiate these structures. In the first of these  $[N,N^{1s},N^B,N^{2s}]$  structures,  $[N,N^{1s},N^B,N^{2s}](1)$ , a hydrogen bond between the terminal carbonyl oxygen and the hydrogenated backbone carbonyl oxygen stabilizes the peptide backbone. The second structure,  $[N,N^{1s},N^B,N^{2s}](2)$ , places the stabilizing hydrogen bond between the terminal carbonyl oxygen and one of the hydrogens attached to the terminal amine group. The third structure,  $[N,N^{1s},N^B,N^{2s}](3)$ , has the stabilizing hydrogen bond placed in between the terminal COH and the hydrogenated CO of the peptide backbone. The MP2 level predicts the  $[N,N^{1s},N^B,N^{2s}](2)$  structure to be the lowest energy, with the  $[N,N^{1s},N^B,N^{2s}](3)$  structure being nearly isoenergetic (<1 kJ/mol difference), with the  $[N,N^{1s},N^B,N^{2s}](3)$  structure 6 kJ/mol higher in energy than the GS. The DFT levels place an energetic penalty (higher in relative 298 K Gibbs energy) on the  $[N,N^{1s},N^B,N^{2s}](1)$  structure of 4 – 10 kJ/mol relative to the DFT GS, whereas the  $[N,N^{1s},N^B,N^{2s}](2)$  and  $[N,N^{1s},N^B,N^{2s}](3)$  structures have penalties of 8 – 17 and 14 – 21 kJ/mol, respectively.

The [N,N<sup>1s</sup>,N<sup>B</sup>,CO] structure was also located, with the DFT levels predicting an energetic penalty of 11 - 15 kJ/mol in comparison to the DFT GS (MP2 places this structure 26 kJ/mol above the MP2 GS). The HisHis ligand again adopts an iminol configuration, coordinating the Zn metal with the terminal amine nitrogen and carboxylic CO, as well as the  $\pi$  nitrogen of the first His residue and the backbone nitrogen. Here, the hydrogen originating from N<sup>B</sup> is located on the  $\pi$  nitrogen of the second His residue (N<sup>2s</sup>), and forms a hydrogen bond with the backbone CO. A second [N<sup>1s</sup>,N<sup>B</sup>,N<sup>2s</sup>,CO](2) structure is similar to the DFT GS but the carboxylic proton is no longer forming a hydrogen bond with the CO, which comes with an energetic penalty of 22 - 25 kJ/mol relative to the GS.

Relative Energies and Structures of Cd Complexes

Structures and relative energies for the  $Cd^{2+}(HisHis)$  complexes are detailed in Table 2 and Figure 3. Here, all explored levels of theory predict that the  $[N^{1s},N^B,N^{2s},CO]$  structure is the GS, which has the same structure as the Zn analogue. The next lowest energy complex is the  $[N,N^{1s},N^B,N^{2s}](1)$ , which the DFT levels predict is 10-15 kJ/mol above the GS, whereas the MP2 predicts a penalty of only 4 kJ/mol. The remaining structures largely mirror those found for the Zn species, with the exceptions of the highest-energy structure,  $[N,N^{1s},CO^B,N^{2s}]$ , which has a charge solvated motif in which the metal coordinates with both  $\pi$  nitrogens of the imidazole sidechains, the terminal amine nitrogen, and the backbone CO. All levels of theory place the charge solvated motif significantly above the GS (24 – 34 kJ/mol), which is consistent with earlier work favoring the iminol structure for the late transition metals.[52]

Relative Energies and Structures of the Cu Complexes

Structures and relative energies for the Cu<sup>2+</sup>(HisHis) complexes are detailed in Table 3 and Figure 4. Several of the structures are similar to their Zn and Cd analogues. As opposed to the Zn and Cd species, which all have singlet spins, the Cu species presented here are doublets. Quartet structures were investigated, but none were low-lying enough in energy to be competitive with the doublet structures. The B3LYP, B3P86, and B3LYP-GD3BJ levels of theory indicate that the [N,N<sup>1s</sup>,N<sup>B</sup>,CO] is the GS. The MP2 level predicts this structure to be 12 kJ/mol higher in energy

than the  $[N,N^{1s},N^B,N^{2s}]$  (1) structure, the MP2 GS. Uniquely, the pentadentate  $[N,N^{1s},N^BH,N^{2s},CO]$  structure was located for the Cu species. This structure is characterized by coordinating the Cu ion with the terminal amine,  $\pi$  nitrogens of both imidazole sidechains, the terminal carboxylic oxygen, and the backbone amide. Importantly, the hydrogen on this backbone nitrogen has not migrated away, thus differing from the iminol structures previously detailed. If this structure is reexamined for the Zn and Cd species, the geometry optimization converted the pentadentate structure into the four-coordinate  $[N,N^{1s},N^B,N^{2s}]$  (1) complex in which the backbone hydrogen has migrated away. The MP2 level predicts this pentadentate structure to be 2 kJ/mol higher in energy than the copper  $[N,N^{1s},N^B,N^{2s}]$  (1) GS.

# IRMPD Spectra of Metalated HisHis Dipeptide

The infrared multiple photon dissociation spectra for the  $Zn^{2+}$ (HisHis),  $Cd^{2+}$ (HisHis), and  $Cu^{2+}$ (HisHis) complexes are shown in Figure 5. The wavelength-dependent fragmentation for each species was reviewed to ensure each fragment matches both the depletion spectra of the reactant and the overall yield spectra. All fragments used in the analysis are tabulated in the Supporting Information, Table S1. In the case of the Zn and Cd species, the dominant fragmentation patterns observed involve water and carbon monoxide loss. The fragmentation mechanism for Cu complexes mirrored that of the Zn and Cd complexes in that water and carbon monoxide loss were observed but were accompanied by loss of OCNH and  $C_4H_6N_2$  (the His side chain) and several charge separation channels, including loss of OCNH $_2$ <sup>+</sup>. The Zn and Cd spectra have many bands in common, suggesting the coordination motifs of those two species are similar. The most intense band for both species is broad and centered at 1670 and 1690 cm $^{-1}$  for Zn and Cd, respectively. The Zn species has a weak band at 1739 cm $^{-1}$  that is not shared with the Cd species, possibly indicating an additional structure is populated. The Cu spectrum appears distinct relative to the Zn and Cd spectra, indicating a new structural motif is being observed. All three species share a band at  $\sim$ 720 cm $^{-1}$ .

Comparison of Experimental and Theoretical Spectra: Zn<sup>2+</sup>(HisHis)

The experimental IRMPD spectrum for Zn<sup>2+</sup>(HisHis) is compared to the theoretical infrared spectra for three low-lying isomers in Figure 6. Major experimental bands are located at 1670, 1165, and 1091 cm<sup>-1</sup>, with minor bands located at 1739, 1583, 1506, 1434 (broad), 1350, and 1280 (broad) cm<sup>-1</sup>. A magnified inset of the spectral region below 1000 cm<sup>-1</sup> highlights the minor experimental bands located at 841, 723, and 684 cm<sup>-1</sup>. The DFT GS, [N<sup>1s</sup>,N<sup>B</sup>,N<sup>2s</sup>,CO](1), recreates several of these experimental bands. This structure predicts vibrational bands at 1674 (CN imine stretch) and 1666 cm<sup>-1</sup> (coordinated CO stretch) that recreate the appearance of the major band at 1670 cm<sup>-1</sup>. The predicted vibration at 1674 cm<sup>-1</sup> is especially characteristic of an iminol structure. The small band at 1583 cm<sup>-1</sup> is assigned to the NH<sub>2</sub> umbrella motion, where the theoretical band is located at 1623 cm<sup>-1</sup>. This motion has been reported to be significantly anharmonic and is often experimentally observed red shifted 20 - 50 cm<sup>-1</sup> in similar metalated amino acid systems.[33, 34, 37-43, 49-51] This experimental band also has some contributions from the imidazole sidechain stretching motions located at 1573 and 1567 cm<sup>-1</sup>, with more of these motions located at 1502 and 1497 cm<sup>-1</sup>, nicely matching the experimental band centered at 1506 cm<sup>-1</sup>. The broad experimental band at 1434 cm<sup>-1</sup> is matched by the backbone CH motions and CO stretch of the uncoordinated carboxylic oxygen predicted at 1428 and 1415 cm<sup>-1</sup>. Below 1200 cm<sup>-1</sup> 1, the theoretically predicted bands for this structure do not reproduce closely the relative intensity of the experimental bands. The experimental band at 1165 cm<sup>-1</sup> is matched in location, if not intensity, by a predicted band at 1174 cm<sup>-1</sup>, which is for the carboxylic acid COH bending motion. The experimental band at 1091 cm<sup>-1</sup> is most closely matched to a predicted vibration at 1083 cm<sup>-1</sup> <sup>1</sup>, which is the result of miscellaneous imidazole ring motions. Below 1000 cm<sup>-1</sup>, minor bands are observed at 840 (backbone COH out-of plane bend), 710 (terminal COH out-of-plane bending), 761 (miscellaneous backbone CH motions), 682 and 679 (out-of-plane bending of the  $N_{\tau}H$  for both His sidechains) cm<sup>-1</sup>. These predicted bands are in reasonable agreement with the observed spectrum.

The DFT GS does not predict the minor band located at 1739 cm<sup>-1</sup>, the intensity of the two peaks at 1165 and 1091 cm<sup>-1</sup>, and the small bands between 1200 – 1400 cm<sup>-1</sup> are poorly

reproduced. Two [N,N<sup>1s</sup>,N<sup>B</sup>,N<sup>2s</sup>] structures are also compared to the experimental IRMPD spectrum in Figure 6. In the case of the [N,N<sup>1s</sup>,N<sup>B</sup>,N<sup>2s</sup>](1) structure, the most intense band is located at 1728 cm<sup>-1</sup> (uncoordinated CO stretch), which agrees nicely with the small experimental band at 1739 cm<sup>-1</sup>. The CN imine stretch and NH<sub>2</sub> scissor motions are now located at 1635 and 1612 cm<sup>-1</sup> <sup>1</sup>, respectively, which do a poorer job of recreating the experimental band at 1670 cm<sup>-1</sup>. For bands between 1300 – 1600 cm<sup>-1</sup>, the [N,N<sup>1s</sup>,N<sup>B</sup>,N<sup>2s</sup>](1) structure recreates these bands with good fidelity, arguably somewhat more poorly than the DFT GS. The [N,N<sup>1s</sup>,N<sup>B</sup>,N<sup>2s</sup>] structures differ from the DFT GS in the hydrogen bonding that stabilizes the backbone of the HisHis dipeptide, such that the [N,N<sup>1s</sup>,N<sup>B</sup>,N<sup>2s</sup>](1) structure predicts a vibration at 1266 cm<sup>-1</sup> for the backbone COH bending mode that recreates the minor, broad experimental feature at 1280 cm<sup>-1</sup> better than the DFT GS. Additionally, the [N,N<sup>1s</sup>,N<sup>B</sup>,N<sup>2s</sup>](1) structure predicts moderately intense bands at 1170 (carboxylic acid COH bending) and 1167 (NH<sub>2</sub> twisting) cm<sup>-1</sup>, as well as at 1099 cm<sup>-1</sup> (NH<sub>2</sub> wagging), which better reproduce the experimental intensities of the two bands between 1000 – 1200 cm<sup>-1</sup>. The [N,N<sup>1s</sup>,N<sup>B</sup>,N<sup>2s</sup>](1) structure predicts bands at 838 (backbone COH out-of plane bend), 744 (miscellaneous backbone CH motions), 681 and 680 (out-of-plane bending of the N<sub>T</sub>H for both His sidechains) cm<sup>-1</sup>, which recreate the minor experimental features shown in the magnified inset (although perhaps not quite as well as the DFT GS).

In comparison to the [N¹s,NB,N²s,CO](1) and [N,N¹s,NB,N²s](1) structures, the [N,N¹s,NB,N²s](2) is a worse match to the experimental spectrum. The predicted bands at 1765 (carboxylic acid stretch) and 1692 (CN imine stretch) cm⁻¹ appear to be blue-shifted compared to the experimental bands. The relative intensities of the bands at 1300 (backbone COH bend) and 1143 (carboxylic acid COH bend) cm⁻¹ do not match the experimental spectrum as well as the two aforementioned structures. The predicted bands at 1765, 1300, and 1143 cm⁻¹ are particularly characteristic for this structure, which does not have the stabilizing hydrogen bond between the carboxylic acid CO and the hydrogenated backbone CO. This last band does not appear in the experimental spectrum, precluding this structure from being included in the experimental conformer population.

Theoretically, the B3LYP and B3P86 levels predict the majority (98 – 96%) of the ions to be the  $[N^{1s},N^B,N^{2s},CO](1)$  conformer, assuming an equilibrium distribution at 298 K. B3LYP-GD3BJ predicts that only 80% of the ions adopt the  $[N^{1s},N^B,N^{2s},CO](1)$  conformation, 16%  $[N,N^{1s},N^B,N^{2s}](1)$ , and the remaining 4%  $[N,N^{1s},N^B,N^{2s}](2)$ . The MP2 level instead favors the  $[N,N^{1s},N^B,N^{2s}]$  structures, with approximately equal amounts predicted to be in the  $[N,N^{1s},N^B,N^{2s}](1)$  and  $[N,N^{1s},N^B,N^{2s}](2)$  conformations (37 and 42%, respectively). The  $[N^{1s},N^B,N^{2s},CO](1)$  structure appears to dominate the experimental ion population according to spectral comparison, with minor contributions from the  $[N,N^{1s},N^B,N^{2s}]$  structures likely, observations that agree best with the prediction made by the B3LYP-GD3BJ level of theory.

Comparison of Experimental and Theoretical Spectra:  $Cd^{2+}(HisHis)$ 

The experimental IRMPD spectrum for Cd<sup>2+</sup>(HisHis) is compared to the theoretical infrared spectra for three low-lying isomers in Figure 7. Experimental bands are located at 1690, 1585, 1500, 1424 (broad), 1348, 1275 (broad), 1214, 1160, 1085, and 679 cm<sup>-1</sup>. The GS at all levels of theory is [N<sup>1s</sup>,N<sup>B</sup>,N<sup>2s</sup>,CO], which provides a good match to the experimental spectrum. Like the Zn analogue, the bands between 1000 – 1200 cm<sup>-1</sup> are more intense than the predicted bands at 1167 and 1078 cm<sup>-1</sup>. In contrast, the broad experimental band centered at 1424 cm<sup>-1</sup> is less intense than predicted.

As opposed to the Zn analogue, the Cd species does not exhibit a discernible band near 1740 cm<sup>-1</sup>. The second lowest energy structure, [N,N<sup>1s</sup>,N<sup>B</sup>,N<sup>2s</sup>](1), has a predicted band at 1724 cm<sup>-1</sup>. The experimental spectrum is non-zero in this region, such that one cannot conclusively rule out a small contribution from this structure in the gas phase. The spectrum for this structure differs from the GS and the experimental spectrum in the range of 1200 – 1800 cm<sup>-1</sup>. In contrast to the GS, the intensities of the experimental peaks at 1085 and 1160 cm<sup>-1</sup> are better reproduced by the theoretical bands at 1080 and 1165 cm<sup>-1</sup> for the [N,N<sup>1s</sup>,N<sup>B</sup>,N<sup>2s</sup>](1) structure. In the [N,N<sup>1s</sup>,N<sup>B</sup>,N<sup>2s</sup>](1) structure, these bands are shifted by only ~2 cm<sup>-1</sup> from the GS, which is beyond the resolution available in this experiment and the accuracy of the DFT calculation.

Figure 7 also includes a comparison between the experimental spectrum and the  $[N,N^{1s},N^B,CO]$  structure, which fails to reproduce numerous experimental features. Further, all levels of theory predict that < 1% of the ion population would adopt this conformation at 298 K. All the DFT levels of theory predict > 99% of the ion population would adopt the  $[N^{1s},N^B,N^{2s},CO]$  conformer, whereas MP2 predicts only 83% would be in the  $[N^{1s},N^B,N^{2s},CO]$  state, with 17% in  $[N,N^{1s},N^B,N^{2s}]$  (1). Here, the experimental ion population appears to be well-predicted by the DFT levels of theory, as the dominant conformer is in  $[N^{1s},N^B,N^{2s},CO]$  motif, although a very small population of  $[N,N^{1s},N^B,N^{2s}]$  (1) cannot be ruled out.

Comparison of Experimental and Theoretical Spectra: Cu<sup>2+</sup>(HisHis)

Figure 8 compares the IRMPD spectrum of Cu<sup>2+</sup>(HisHis) with the three lowest-lying structures. Experimental bands are present at 1639, 1594, 1381 (broad), 1265, 1136, 1080, 682, and 611 cm<sup>-1</sup> along with a minor band at 1745 cm<sup>-1</sup> shown in the inset. For the DFT GS, [N,N<sup>1s</sup>,N<sup>B</sup>,CO], the metal-coordinated CO stretch at 1641 cm<sup>-1</sup> and hydrogen-bonded CO stretch at 1647 cm<sup>-1</sup> recreate the experimental band at 1639 cm<sup>-1</sup>. The experimental band at 1594 cm<sup>-1</sup> is predicted by theoretical bands at 1607 and 1601 cm<sup>-1</sup>, which are assigned to the CC stretching mode of the second His residue imidazole moiety and the NH<sub>2</sub> scissor motion, respectively. Three major theoretical bands appear to closely resemble the broad experimental band at 1381 cm<sup>-1</sup>. The mode at 1417 cm<sup>-1</sup> is the in-plane rocking motion of the  $N_{\pi}H$  of the second His residue, the mode at 1405 cm<sup>-1</sup> is the CO stretch of the uncoordinated oxygen of the terminal carboxylic acid, and the mode at 1380 cm<sup>-1</sup> is the metal coordinated CN imine stretch. Two moderately intense bands are predicted near the experimental band centered at 1136 cm<sup>-1</sup>. The first is at 1178 cm<sup>-1</sup>, which is for the imidazole in-plane rocking motion and lies slightly outside the experimental band. At 1139 cm<sup>-1</sup>, the first His  $N_{\pi}H$  and  $N_{\tau}H$  in-plane bending motions are found. A predicted band at 1079 cm<sup>-1</sup> <sup>1</sup> from the first His residue imidazole in-plane rocking matches the band observed at 1080 cm<sup>-1</sup>, but several predicted bands of comparable intensity at lower wavenumber are not observed. The sharp experimental bands at 682 and 611 cm<sup>-1</sup> are in a spectral region where the predicted structure has several out-of-plane imidazole modes, but none that are intense or sharp as the experimental features.

The MP2 GS, [N,N<sup>1s</sup>,N<sup>B</sup>,N<sup>2s</sup>](1), is also compared to the IRMPD spectrum in Figure 8, and produces a less satisfying match than the DFT GS in the higher frequency range. Two intense bands are predicted at 1761 and 1686 cm<sup>-1</sup> for the uncoordinated CO stretch of the carboxylic acid group and the metal coordinated CN imine stretch, respectively. The experimental spectrum has evidence for a very small, resolved band at 1745 cm<sup>-1</sup>, but not near 1690 cm<sup>-1</sup> in this spectral range. No band is predicted that matches the experimental band at 1639 cm<sup>-1</sup>, but there is a predicted band at 1603 cm<sup>-1</sup> (NH<sub>2</sub> scissor mode) that could match with the experimental band at 1594 cm<sup>-1</sup>. Between 1500 – 1200 cm<sup>-1</sup>, the predicted bands at 1497 and 1493 cm<sup>-1</sup> (miscellaneous imidazole rocking) seem to match with a very minor band centered at 1498 cm<sup>-1</sup>, and the broad experimental band centered at 1381 cm<sup>-1</sup> matches better with the theoretical bands at 1394 and 1365 cm<sup>-1</sup> (miscellaneous backbone CH motions). An intense band is located at 1300 cm<sup>-1</sup> (backbone COH motions), which is blue-shifted from the small experimental band at 1265 cm<sup>-1</sup>. The MP2 GS does predict a band at 1145 cm<sup>-1</sup> (terminal COH bending) that matches the experimental band at 1136 cm<sup>-1</sup>. This structure also predicts two sharp peaks below 700 cm<sup>-1</sup> (676 and 672 cm<sup>-1</sup> for the outof-plane bending of the N<sub>τ</sub>H for both His sidechains; 611 cm<sup>-1</sup> for the terminal COH out-of-plane bending) that matches the experimental spectrum better than the DFT GS.

Finally, the pentadentate [N,N<sup>1s</sup>,N<sup>B</sup>H,N<sup>2s</sup>,CO] conformer is compared to the experimental spectrum in Figure 8. The predicted band at 1762 cm<sup>-1</sup> is assigned to the backbone CO stretching motion and could explain the very small band near 1740 cm<sup>-1</sup>. The most intense predicted band is located at 1651 cm<sup>-1</sup> (terminal coordinated CO stretch), and along with the 1601 cm<sup>-1</sup> predicted band (NH<sub>2</sub> scissor), seems to match the position of the experimental bands in that range, but not their intensities relative to one another or the rest of the spectrum. The terminal COH bend is predicted to be at 1174 cm<sup>-1</sup>, potentially matching the blue shoulder of the 1136 cm<sup>-1</sup> experiment peak. The red shoulder of this experimental peak appears to capture the predicted band at 1084

cm<sup>-1</sup> (NH<sub>2</sub> wagging) better than the other two low-lying conformers. Below 700 cm<sup>-1</sup>, predicted bands appear at 678, 677, and 615 cm<sup>-1</sup> that match the aforementioned modes of the MP2 GS.

Because of the sizeable energetic penalties, the theoretical single point energies predicted by all three DFT methods indicate that [N,N<sup>1s</sup>,N<sup>B</sup>,CO] should comprise 98 – 99% of the ion population in an equilibrium distribution of conformers at 298 K, with the B3LYP-GD3BJ predicting a small population (< 2%) adopting the [N,N<sup>1s</sup>,N<sup>B</sup>,N<sup>2s</sup>](1) conformation. The MP2 prediction contrasts this result by predicting that < 1% of the ions adopt the [N,N<sup>1s</sup>,N<sup>B</sup>,CO] structure, with 69% being in the [N,N<sup>1s</sup>,N<sup>B</sup>,N<sup>2s</sup>](1) conformation, and the remainder (30%) in the pentadentate [N,N<sup>1s</sup>,N<sup>B</sup>H,N<sup>2s</sup>,CO]. From a spectral comparison, it is difficult to assign the presence of the [N,N<sup>1s</sup>,N<sup>B</sup>,N<sup>2s</sup>](1) and [N,N<sup>1s</sup>,N<sup>B</sup>H,N<sup>2s</sup>,CO] structures because of the lack of significant evidence of the predicted bands above 1650 cm<sup>-1</sup>, even though a mix of the two structures could explain the features below 1650 cm<sup>-1</sup>. The DFT GS does not seem to accurately predict the two sharp experimental bands below 700 cm<sup>-1</sup>, but does match several spectral features, particularly in regards to the CO stretching modes. Therefore, we conclude that [N,N<sup>1s</sup>,N<sup>B</sup>,CO] is present, with possibly small contributions from [N,N<sup>1s</sup>,N<sup>B</sup>,N<sup>2s</sup>](1) and [N,N<sup>1s</sup>,N<sup>B</sup>H,N<sup>2s</sup>,CO] structures.

### **Conclusions**

The IRMPD spectra of  $Zn^{2+}$  (HisHis),  $Cd^{2+}$  (HisHis), and  $Cu^{2+}$  (HisHis) have been presented. Comparisons to theoretical spectra have identified the dominant coordination motifs for the Zn and Cd species. Both species exhibit characteristics bands for a structure that coordinates the divalent metal ion with both  $\pi$  nitrogens of the imidazole sidechains, the terminal carbonyl oxygen, and the backbone nitrogen (which has displaced its hydrogen atom), which is denoted as the  $[N^{1s},N^B,N^{2s},CO]$  conformer. In the case of Zn, there is a possible second conformer present that coordinates the metal ion with the amino nitrogen, both sidechain  $\pi$  nitrogens, and the backbone nitrogen, denoted as  $[N,N^{1s},N^B,N^{2s}]$ . In the case of Cd, this second conformation is less obviously present and is not necessary to explain all spectral features. The Cu system was more difficult to assign to a single structure, and instead likely consists of the  $[N,N^{1s},N^B,CO]$  structure with

contributions from the [N,N¹s,NB,N²s] and [N,N¹s,NBH,N²s,CO] conformers. The Zn and Cd species share similar coordination motifs, which is not unexpected given their similar ionic character, whereas Cu has a separate binding profile that could explain why cross-linking of amyloid-β-peptides is inhibited by the addition of Cu(II).[5] Although this characteristic binding profile could not be unambiguously assigned using the methods presented here, a subsequent investigation can be envisioned utilizing H/D exchange and highly accurate mass measurements, as were used to determine the structure of cyclic peptides complexed with copper.[53] Energetically, the DFT methods used here (B3LYP, B3P86, and B3LYP-GD3BJ) predict the dominant conformers of the Zn and Cd species with better performance than the MP2 level. In the case of Cu, the disagreement between the DFT and MP2 energies was more pronounced.

## Acknowledgments

Financial support for this work was provided by the National Science Foundation, Grants CHE-2313553. The authors appreciatively acknowledge the *Nederlandse Organisatie voor Wetenschappelijk Onderzoek* (NWO) for the support of the FELIX Laboratory and a generous grant of computer time from the Center of High Performance Computing at the University of Utah.

### References

- [1] W.P. Esler, E.R. Stimson, J.M. Jennings, J.R. Ghilardi, P.W. Mantyh, J.E. Maggio, Zincinduced aggregation of human and rat  $\beta$ -amyloid peptides in vitro, J. Neurochem., 66 (1996) 723-732.
- [2] A.I. Bush, W.H. Pettingell, G. Multhaup, M. d Paradis, J.-P. Vonsattel, J.F. Gusella, K. Beyreuther, C.L. Masters, R.E. Tanzi, Rapid induction of Alzheimer Aβ amyloid formation by zinc, Science, 265 (1994) 1464-1467.
- [3] C. Cragnell, L. Staby, S. Lenton, B.B. Kragelund, M. Skepö, Dynamical oligomerisation of histidine rich intrinsically disordered proteins is regulated through zinc-histidine interactions, Biomolecules, 9 (2019) 168.
- [4] A.N. Istrate, S.A. Kozin, S.S. Zhokhov, A.B. Mantsyzov, O.I. Kechko, A. Pastore, A.A. Makarov, V.I. Polshakov, Interplay of histidine residues of the Alzheimer's disease Aβ peptide governs its Zn-induced oligomerization, Sci. Rep., 6 (2016) 1-14.
- [5] K. Suzuki, T. Miura, H. Takeuchi, Inhibitory effect of copper (II) on zinc (II)-induced aggregation of amyloid β-peptide, Biochem. Biophys. Res. Commun., 285 (2001) 991-996.

- [6] J. Miller, A. McLachlan, A. Klug, Repetitive zinc-binding domains in the protein transcription factor IIIA from Xenopus oocytes, EMBO J., 4 (1985) 1609-1614.
- [7] J.P. Mackay, M. Crossley, Zinc Fingers are Sticking Together, Trends Biochem. Sci., 23 (1998) 1-4.
- [8] G. Malgieri, M. Palmieri, S. Esposito, V. Maione, L. Russo, I. Baglivo, I. de Paola, D. Milardi, D. Diana, L. Zaccaro, P.V. Pedone, R. Fattorusso, C. Isernia, Zinc to cadmium replacement in the prokaryotic zinc-finger domain, Metallomics, 6 (2014) 96-104.
- [9] G. Malgieri, L. Zaccaro, M. Leone, E. Bucci, S. Esposito, I. Baglivo, A.D. Gatto, L. Russo, R. Scandurra, P.V. Pedone, R. Fattorusso, C. Isernia, Zinc to cadmium replacement in the A. thaliana SUPERMAN Cys<sub>2</sub>His<sub>2</sub> zinc finger induces structural rearrangements of typical DNA base determinant positions, Biopolymers, 95 (2011) 801-810.
- [10] P.F. Predki, B. Sarkar, Effect of replacement of "zinc finger" zinc on estrogen receptor DNA interactions, J. Biol. Chem., 267 (1992) 5842-5846.
- [11] D. Petering, M. Huang, S. Moteki, C. Shaw III, Cadmium and lead interactions with transcription factor IIIA from Xenopus laevis: a model for zinc finger protein reactions with toxic metal ions and metallothionein, Mar. Environ. Res., 50 (2000) 89-92.
- [12] M. Huang, D. Krepkiy, W. Hu, D.H. Petering, Zn-, Cd-, and Pb-transcription factor IIIA: properties, DNA binding, and comparison with TFIIIA-finger 3 metal complexes, J. Inorg. Biochem., 98 (2004) 775-785.
- [13] R. Kothinti, A. Blodgett, N.M. Tabatabai, D.H. Petering, Zinc finger transcription factor Zn3-Sp1 reactions with Cd2+, Chem. Res. Toxicol., 23 (2010) 405-412.
- [14] D. Krepkiy, F.H. Försterling, D.H. Petering, Interaction of Cd2+ with Zn finger 3 of transcription factor IIIA: structures and binding to cognate DNA, Chem. Res. Toxicol., 17 (2004) 863-870.
- [15] J. Oomens, N.C. Polfer, G. Berden, J.R. Eyler, Gas-phase metal ion chelation investigated with IRMPD spectroscopy: A brief review of Robert Dunbar's contributions, Eur. J. Mass Spectrom., 25 (2019) 86-96.
- [16] R.C. Dunbar, G. Berden, J.K. Martens, J. Oomens, Divalent Metal-Ion Complexes with Dipeptide Ligands Having Phe and His Side-Chain Anchors: Effects of Sequence, Metal Ion, and Anchor, J. Phys. Chem. A, 119 (2015) 9901-9909.
- [17] R.C. Dunbar, J. Martens, G. Berden, J. Oomens, Transition Metal(II) Complexes of Histidine-containing Tripeptides: Structures, and Infrared Spectroscopy by IRMPD, Int. J Mass Spectrom., 429 (2018) 198-205.
- [18] D. Oepts, A.F.G. van der Meer, P.W. van Amersfoort, The Free-Electron-Laser User Facility FELIX, Infrared Phys. Technol., 36 (1995) 297-308.
- [19] J. Martens, G. Berden, C.R. Gebhardt, J. Oomens, Infrared ion spectroscopy in a modified quadrupole ion trap mass spectrometer at the FELIX free electron laser laboratory, Rev. Sci. Instrum., 87 (2016) 103108.
- [20] G. Berden, M. Derksen, K.J. Houthuijs, J. Martens, J. Oomens, An Automatic Variable Laser Attenuator for IRMPD Spectroscopy and Analysis of Power-dependence in Fragmentation Spectra, Int. J. Mass Spectrom., 443 (2019) 1-8.
- [21] J. Lemaire, P. Boissel, M. Heninger, G. Mauclaire, G. Bellec, H. Mestdagh, S. Le Caer, J. Ortega, F. Glotin, P. Maître, Gas Phase Infrared Spectroscopy of Selectively Prepared Ions, Phys. Rev. Lett., 89 (2002) 273002.
- [22] C.P. McNary, P.B. Armentrout, Threshold Collision-Induced Dissociation of Proton-Bound Hydrazine and Dimethylhydrazine Clusters, J. Phys. Chem. A, 120 (2016) 9690-9701.

- [23] C.P. McNary, Y.-w. Nei, P. Maitre, M.T. Rodgers, P.B. Armentrout, Infrared Multiple Photon Dissociation Spectroscopy of Protonated Glycine, Lysine, Histidine, and Arginine Complexed with 18-Crown-6, Phys. Chem. Chem. Phys., 21 (2019) 12625-12639. [24] R.M. Moision, P.B. Armentrout, The Special Five-membered Ring of Proline: An Experimental and Theoretical Investigation of Alkali Metal Cation Interactions with Proline and Its Four- and Six-membered Ring Analogues, J. Phys. Chem. A, 110 (2006) 3933-3946. [25] D.A. Case, V. Babin, J.T. Berryman, R.M. Betz, Q. Cai, D.S. Cerutti, T.E. Cheatham, T.A. Darden, R.E. Duke, H. Gohlke, A.W. Goetz, S. Gusarov, N. Homeyer, P. Janowski, J. Kaus, I. Kolossváry, A. Kovalenko, T.S. Lee, S. LeGrand, T. Luchko, R. Luo, B. Madej, K.M. Merz, F.
- Kolossváry, A. Kovalenko, T.S. Lee, S. LeGrand, T. Luchko, R. Luo, B. Madej, K.M. Merz, F. Paesani, D.R. Roe, A. Roitberg, C. Sagui, R. Salomon-Ferrer, G. Seabra, C.L. Simmerling, W. Smith, J. Swails, R.C. Walker, J. Wang, R.M. Wolf, X. Wu, P.A. Kollman, AMBER 14, in, University of California, San Francisco, 2014.
- [26] M. Valiev, E.J. Bylaska, N. Govind, K. Kowalski, T.P. Straatsma, H.J.J. Van Dam, D. Wang, J. Nieplocha, E. Apra, E. al., NWChem: A comprehensive and scalable open-source solution for large scale molecular simulations, Comput. Phys. Commun., 181 (2010) 1477-1489. [27] M.J. Frisch, G.W. Trucks, H.B. Schlegel, G.E. Scuseria, M.A. Robb, J.R. Cheeseman, G. Scalmani, V. Barone, G.A. Petersson, H. Nakatsuji, X. Li, M. Caricato, A.V. Marenich, J. Bloino, B.G. Janesko, R. Gomperts, B. Mennucci, H.P. Hratchian, J.V. Ortiz, A.F. Izmaylov, J.L. Sonnenberg, D. Williams-Young, F. Ding, F. Lipparini, F. Egidi, J. Goings, B. Peng, A. Petrone, T. Henderson, D. Ranasinghe, V.G. Zakrzewski, J. Gao, N. Rega, G. Zheng, W. Liang, M. Hada, M. Ehara, K. Toyota, R. Fukuda, J. Hasegawa, M. Ishida, T. Nakajima, Y. Honda, O. Kitao, H. Nakai, T. Vreven, K. Throssell, J. J. A. Montgomery, J.E. Peralta, F. Ogliaro, M.J. Bearpark, J.J. Heyd, E.N. Brothers, K.N. Kudin, V.N. Staroverov, T.A. Keith, R. Kobayashi, J. Normand, K. Raghavachari, A.P. Rendell, J.C. Burant, S.S. Iyengar, J. Tomasi, M. Cossi, J.M. Millam, M. Klene, C. Adamo, R. Cammi, J.W. Ochterski, R.L. Martin, K. Morokuma, O. Farkas, J.B. Foresman, D.J. Fox, Gaussian 16, Revision A.03, in, Gaussian, Inc., Wallingford CT, 2016. [28] B.P. Pritchard, D. Altarawy, B. Didier, T.D. Gibson, T.L. Windus, A New Basis Set Exchange: An Open, Up-to-date Resource for the Molecular Sciences Community, J. Chem. Inf. Model., 59 (2019) 4814-4820.
- [29] S. Grimme, S. Ehrlich, L. Goerigk, Effect of the Damping Function in Dispersion Corrected Density Functional Theory, J. Comput. Chem., 32 (2011) 1456-1465.
- [30] S. Grimme, J. Antony, S. Ehrlich, H. Krieg, A Consistent and Accurate Ab Initio Parametrization of Density Functional Dispersion Correction (DFT-D) for the 94 Elements H-Pu, J. Chem. Phys., 132 (2010) 154104-154119.
- [31] M.K. Kesharwani, B. Brauer, J.M.L. Martin, Frequency and Zero-Point Vibrational Energy Scale Factors for Double-Hybrid Density Functionals (and Other Selected Methods): Can Anharmonic Force Fields Be Avoided?, J. Phys. Chem. A, 119 (2015) 1701-1714.
- [32] N.C. Polfer, Infrared Multiple Photon Dissociation Spectroscopy of Trapped Ions, Chem. Soc. Rev., 40 (2011) 2211–2221.
- [33] P.B. Armentrout, M.T. Rodgers, J. Oomens, J.D. Steill, Infrared Multiphoton Dissociation Spectroscopy of Cationized Serine: Effects of Alkali-Metal Cation Size on Gas-Phase Conformation, J. Phys. Chem. A, 112 (2008) 2248-2257.
- [34] M.T. Rodgers, P.B. Armentrout, J. Oomens, J.D. Steill, Infrared Multiphoton Dissociation Spectroscopy of Cationized Threonine: Effects of Alkali-Metal Cation Size on Gas-Phase Conformation, J. Phys. Chem. A, 112 (2008) 2258-2267.

- [35] A.L. Heaton, V.N. Bowman, J. Oomens, J.D. Steill, P.B. Armentrout, Infrared Multiple Photon Dissociation Spectroscopy of Cationized Asparagine: Effects of Metal Cation Size on Gas-Phase Conformation, J. Phys. Chem. A, 113 (2009) 5519-5530.
- [36] D.R. Carl, T.E. Cooper, J. Oomens, J.D. Steill, P.B. Armentrout, Infrared Multiple Photon Dissociation Spectroscopy of Cationized Methionine: Effects of Alkali-Metal Cation Size on Gas-Phase Conformation, Phys. Chem. Chem. Phys., 12 (2010) 3384-3398.
- [37] M. Citir, E.M.S. Stennett, J. Oomens, J.D. Steill, M.T. Rodgers, P.B. Armentrout, Infrared Multiple Photon Dissociation Spectroscopy of Cationized Cysteine: Effects of Metal Cation Size on Gas-Phase Conformation, Int. J. Mass Spectrom., 297 (2010) 9-17.
- [38] T.E. Hofstetter, C. Howder, G. Berden, J. Oomens, P.B. Armentrout, Structural Elucidation of Biological and Toxicological Complexes: Investigation of Monomeric and Dimeric Complexes of Histidine with Multiply Charged Transition Metal (Zn and Cd) Cations using IR Action Spectroscopy, J. Phys. Chem. B, 115 (2011) 12648-12661.
- [39] R.A. Coates, C.P. McNary, G.C. Boles, G. Berden, J. Oomens, P.B. Armentrout, Structural Characterization of Gas-Phase Cysteine and Cysteine Methyl Ester Complexes with Zinc and Cadmium Dications by Infrared Multiple Photon Dissociation Spectroscopy, Phys. Chem. Chem. Phys., 17 (2015) 25799-25808.
- [40] G.C. Boles, R.A. Coates, G. Berden, J. Oomens, P.B. Armentrout, Experimental and Theoretical Investigations of Infrared Multiple Photon Dissociation Spectra of Glutamine Complexes with Zn<sup>2+</sup> and Cd<sup>2+</sup>, J. Phys. Chem. B, 119 (2015) 11607–11617.
- [41] R.A. Coates, G.C. Boles, C.P. McNary, G. Berden, J. Oomens, P.B. Armentrout, Zn<sup>2+</sup> and Cd<sup>2+</sup> Cationized Serine Complexes: Infrared Multiple Photon Dissociation Spectroscopy and Density Functional Theory Investigations, Phys. Chem. Chem. Phys., 18 (2016) 22434 22445.
- [42] G.C. Boles, R.A. Coates, G. Berden, J. Oomens, P.B. Armentrout, Experimental and Theoretical Investigations of Infrared Multiple Photon Dissociation Spectra of Asparagine Complexes with Zn<sup>2+</sup> and Cd<sup>2+</sup> and Their Deamidation Processes, J. Phys. Chem. B, 120 (2016) 12486-12500.
- [43] G.C. Boles, C.J. Owen, G. Berden, J. Oomens, P.B. Armentrout, Experimental and Theoretical Investigations of Infrared Multiple Photon Dissociation Spectra of Glutamic Acid Complexes with Zn<sup>2+</sup> and Cd<sup>2+</sup>, Phys. Chem. Chem. Phys., 19 (2017) 12394 12406.
- [44] G.C. Boles, R.L. Hightower, R.A. Coates, C.P. McNary, G. Berden, J. Oomens, P.B. Armentrout, Experimental and Theoretical Investigations of Infrared Multiple Photon Dissociation Spectra of Aspartic Acid Complexes with Zn<sup>2+</sup> and Cd<sup>2+</sup>, J. Phys. Chem. B, 122 (2018) 3836-3853.
- [45] A.M. Chalifoux, G.C. Boles, G. Berden, J. Oomens, P.B. Armentrout, Experimental and Theoretical Investigations of Infrared Multiple Photon Dissociation Spectra of Arginine Complexes with Zn<sup>2+</sup> and Cd<sup>2+</sup>, Phys. Chem. Chem. Phys., 20 (2018) 20712-20725.
- [46] C.J. Owen, G.C. Boles, G. Berden, J. Oomens, P.B. Armentrout, Experimental and Theoretical Investigations of Infrared Multiple Photon Dissociation Spectra of Lysine Complexes with Zn<sup>2+</sup> and Cd<sup>2+</sup>, Eur. J. Mass Spectrom., 25 (2019) 97-111.
- [47] G.C. Boles, R.L. Hightower, G. Berden, J. Oomens, P.B. Armentrout, Zinc and Cadmium Complexation of l-Threonine: An Infrared Multiple Photon Dissociation Spectroscopy and Theoretical Study, J. Phys. Chem. B, 123 (2019) 9343-9354.
- [48] G.C. Boles, B.C. Stevenson, R.L. Hightower, G. Berden, J. Oomens, P.B. Armentrout, Zinc and cadmium complexation of L-methionine: An infrared multiple photon dissociation spectroscopy and theoretical study, J. Mass Spectrom., 56 (2021) e4580.

- [49] B.C. Stevenson, J. Martens, G. Berden, J. Oomens, M. Schäfer, P.B. Armentrout, IRMPD Spectroscopic and Theoretical Structural Investigations of Zinc and Cadmium Dications Bound to Histidine Dimers, J. Phys. Chem. A, 124 (2020) 10266-10276.
- [50] B.C. Stevenson, K. Peckelsen, J. Martens, G. Berden, J. Oomens, M. Schäfer, P.B. Armentrout, An investigation of inter-ligand coordination and flexibility: IRMPD spectroscopic and theoretical evaluation of calcium and nickel histidine dimers, J. Mol. Spectrosc., 381 (2021) 111532.
- [51] M. Citir, C.S. Hinton, J. Oomens, J.D. Steill, P.B. Armentrout, Infrared Multiple Photon Dissociation Spectroscopy of Cationized Histidine: Effects of Metal Cation Size on Gas-Phase Conformation, J. Phys. Chem. A, 116 (2012) 1532-1541.
- [52] R.C. Dunbar, J.D. Steill, N.C. Polfer, G. Berden, J. Oomens, Peptide Bond Tautomerization Induced by Divalent Metal Ions: Characterization of the Iminol Configuration, Angew. Chem. Int. Ed., 51 (2012) 4591-4593.
- [53] C. Afonso, J.C. Tabet, G. Giorgi, F. Tureček, Gas-phase doubly charged complexes of cyclic peptides with copper in+ 1,+ 2 and+ 3 formal oxidation states: formation, structures and electron capture dissociation, J. Mass Spectrom., 47 (2012) 208-220.

**Table 1.** Relative Gibbs Energies at 298 K (kJ/mol) of Low-Lying Zn<sup>2+</sup>(HisHis) Complexes<sup>a</sup> (0 K energies in parentheses)

Structure	B3LYP	B3P86	B3LYP-GD3BJ <sup>b</sup>	MP2
$[N^{1s},N^{B},N^{2s},CO](1)$	0.0 (0.0)	0.0 (0.0)	0.0 (0.0)	1.7 (2.5)
$[N,N^{1s},N^{B},N^{2s}](1)$	9.7 (8.7)	8.3 (7.2)	4.0 (2.5)	0.3 (0.0)
$[N,N^{1s},N^{B},N^{2s}](2)$	15.2 (16.2)	17.3 (18.4)	7.6 (8.6)	0.0 (1.8)
$[N,N^{1s},N^{B},N^{2s}](3)$	20.1 (20.0)	21.2 (21.1)	13.6 (13.0)	5.9 (6.6)
$[N,N^{1s},N^{B},CO]$	11.5 (13.9)	12.7 (15.0)	15.3 (17.0)	26.4 (29.5)
$[N^{1s},N^{B},N^{2s},CO](2)$	22.8 (23.0)	22.5 (22.6)	22.3 (22.4)	25.2 (26.0)

<sup>a</sup>Calculated at the level of theory specified using a 6-311+G(2d,2p) basis set and B3LYP/6-311+G(d,p) geometries. <sup>b</sup>Calculated using B3LYP-GD3BJ optimized geometries (B3LYP-Gd3BJ/6-311+G(2d,2p)//B3LYP-GD3BJ/6-311+G(d,p)).

**Table 2.** Relative Gibbs Energies at 298 K (kJ/mol) of Low-Lying Cd<sup>2+</sup>(HisHis) Complexes<sup>a</sup> (0 K energies in parentheses)

Structure	B3LYP	B3P86	B3LYP-GD3BJ <sup>b</sup>	MP2
$\boxed{ [N^{1s},N^B,N^{2s},CO] }$	0.0 (0.0)	0.0 (0.0)	0.0 (0.0)	0.0 (0.0)
$[N,N^{1s},N^{B},N^{2s}](1)$	15.1 (13.0)	14.1 (12.1)	10.5 (7.5)	4.0 (1.9)
$[N,N^{1s},N^{B},CO]$	12.6 (12.2)	13.8 (13.3)	16.1 (14.9)	26.4 (26.0)
$[N,N^{1s},N^{B},N^{2s}](2)$	21.2 (23.1)	23.8 (25.7)	16.5 (16.8)	8.7 (10.6)
$[N,N^{1s},N^{B},N^{2s}](3)$	23.5 (22.8)	25.4 (24.7)	18.4 (16.7)	9.6 (8.9)
$[\mathrm{N,}\mathrm{N^{1s},}\mathrm{CO^{B},}\mathrm{N^{2s}}]$	30.1 (28.0)	33.5 (31.4)	25.3 (22.4)	23.9 (21.8)

<sup>a</sup>Calculated at the level of theory specified using a def2-TZVPP basis set and B3LYP/def2-TZVP geometries. <sup>b</sup>Calculated using B3LYP-GD3BJ optimized geometries (B3LYP-GD3BJ/def2-TZVP//B3LYP-GD3BJ/def2-TZVPP).

**Table 3.** Relative Gibbs Energies at 298 K (kJ/mol) of Low-Lying Cu<sup>2+</sup>(HisHis) Complexes<sup>a</sup> (0 K energies in parentheses)

Structure	B3LYP	B3P86	$B3LYP-GD3BJ^b$	MP2
[N,N <sup>1s</sup> ,N <sup>B</sup> ,CO]	0.0 (0.0)	0.0 (0.0)	0.0 (0.0)	12.1 (14.1)
$[N,N^{1s},N^{B},N^{2s}](1)$	21.2 (23.7)	22.0 (24.5)	10.0 (12.8)	0.0 (4.5)
$[\mathrm{N,}\mathrm{N^{1s},}\mathrm{N^{B}H,}\mathrm{N^{2s},}\mathrm{CO}]$	41.2 (37.2)	37.4 (33.4)	14.0 (11.5)	2.0 (0.0)
$[N^{1s},N^B,N^{2s},CO]$	17.5 (17.8)	18.1 (18.4)	12.7 (13.3)	8.3 (10.6)
$[N,N^{1s},N^{B},N^{2s}](2)$	23.4 (22.5)	21.8 (20.9)	14.7 (13.6)	6.4 (7.6)
$[N,N^{1s},N^{B},N^{2s}](3)$	30.9 (31.0)	32.0 (32.1)	21.1 (21.2)	8.8 (11.0)

<sup>a</sup>Calculated at the level of theory specified using a 6-311+G(2d,2p) basis set and B3LYP/6-311+G(d,p) geometries. <sup>b</sup>Calculated using B3LYP-GD3BJ optimized geometries (B3LYP-GD3BJ/6-311+G(2d,2p)//B3LYP-GD3BJ/6-311+G(d,p)).

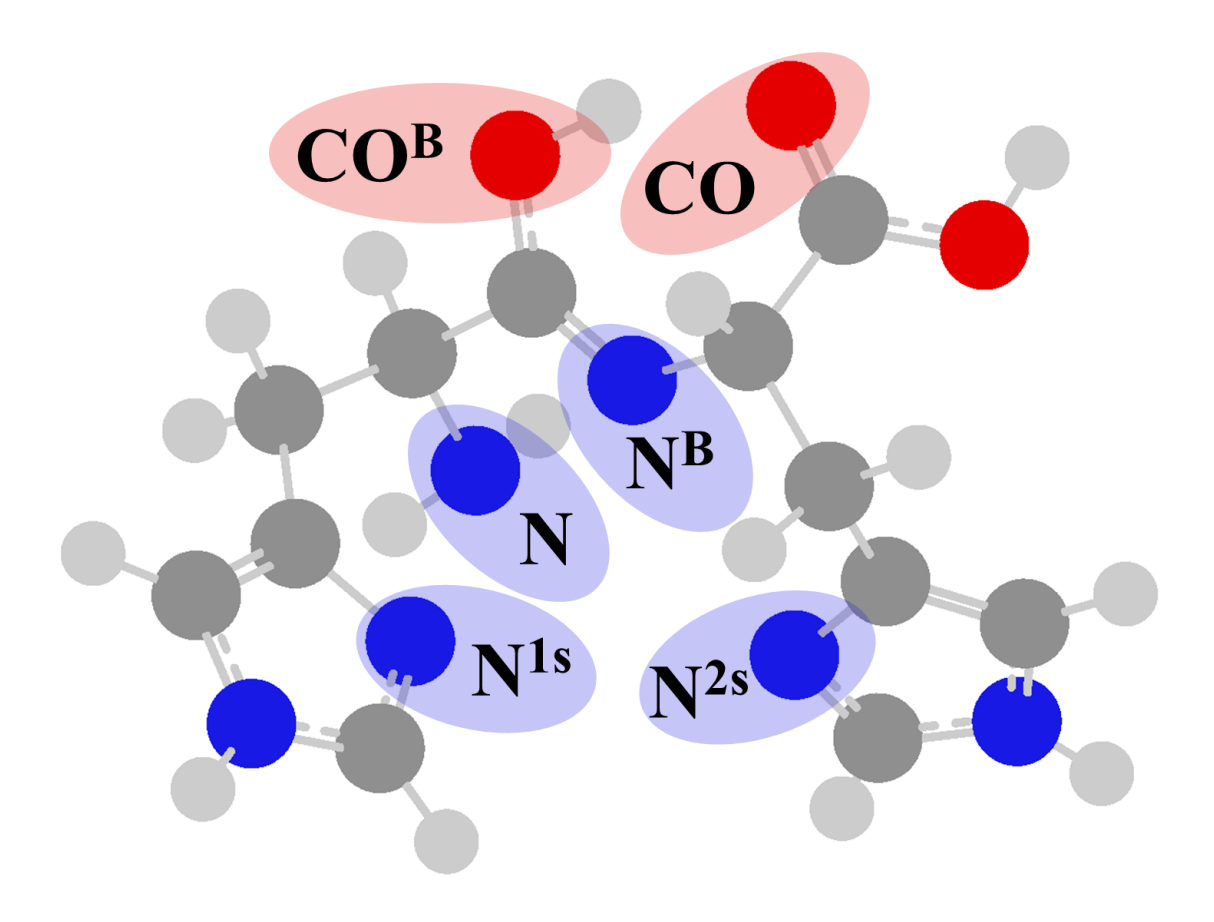


**Figure 1.** Illustration of the nomenclature used to describe the M<sup>2+</sup>(HisHis) complexes and their metal coordination sites. Red—oxygen, grey—carbon, white—hydrogen, blue—nitrogen.

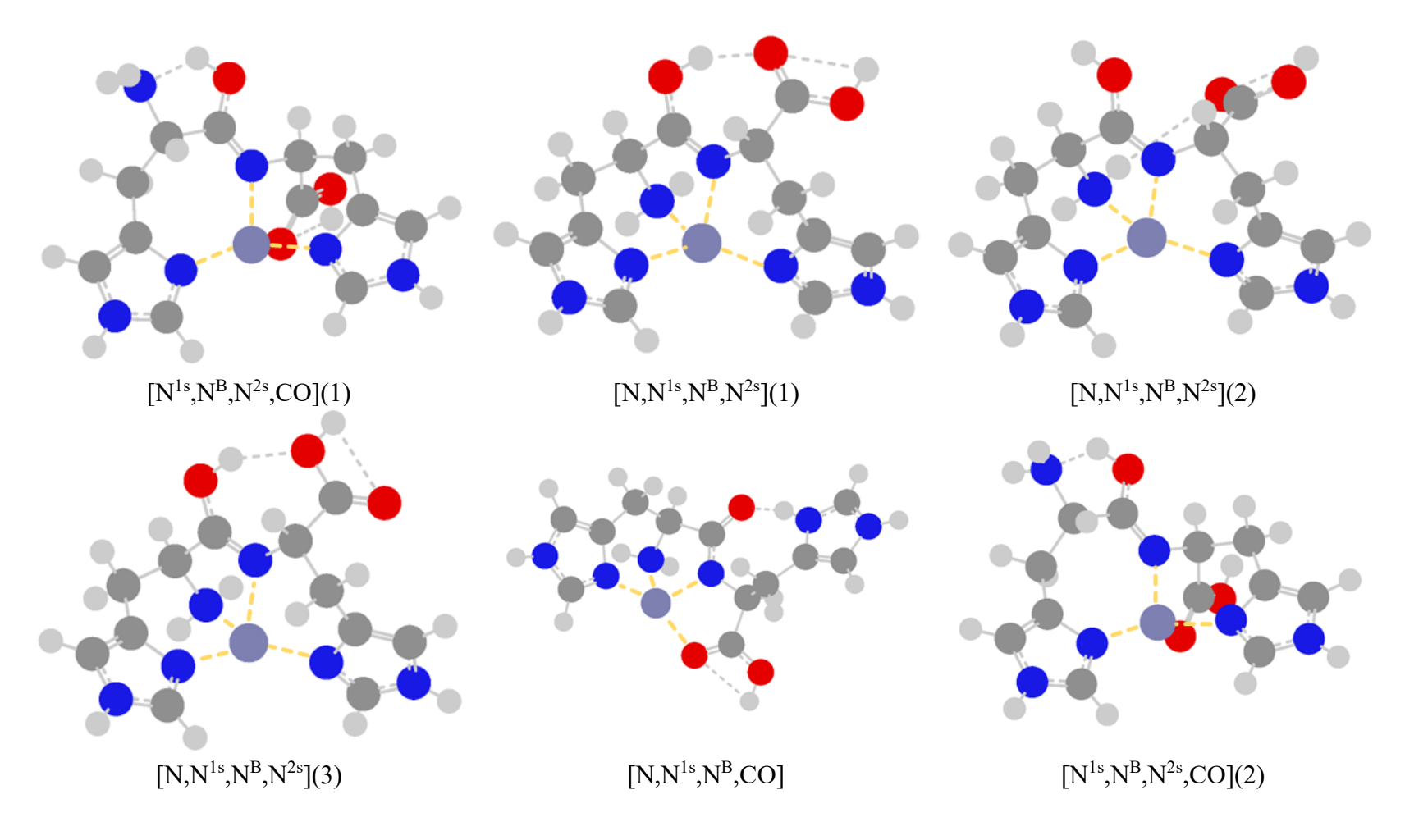


**Figure 2.** Structures of select Zn<sup>2+</sup>(HisHis) conformers calculated at the B3LYP/6-311+G(d,p) level of theory. Red—oxygen, grey—carbon, white—hydrogen, blue—nitrogen, pale blue—zinc. Yellow dashed lines represent metal – ligand bonds.

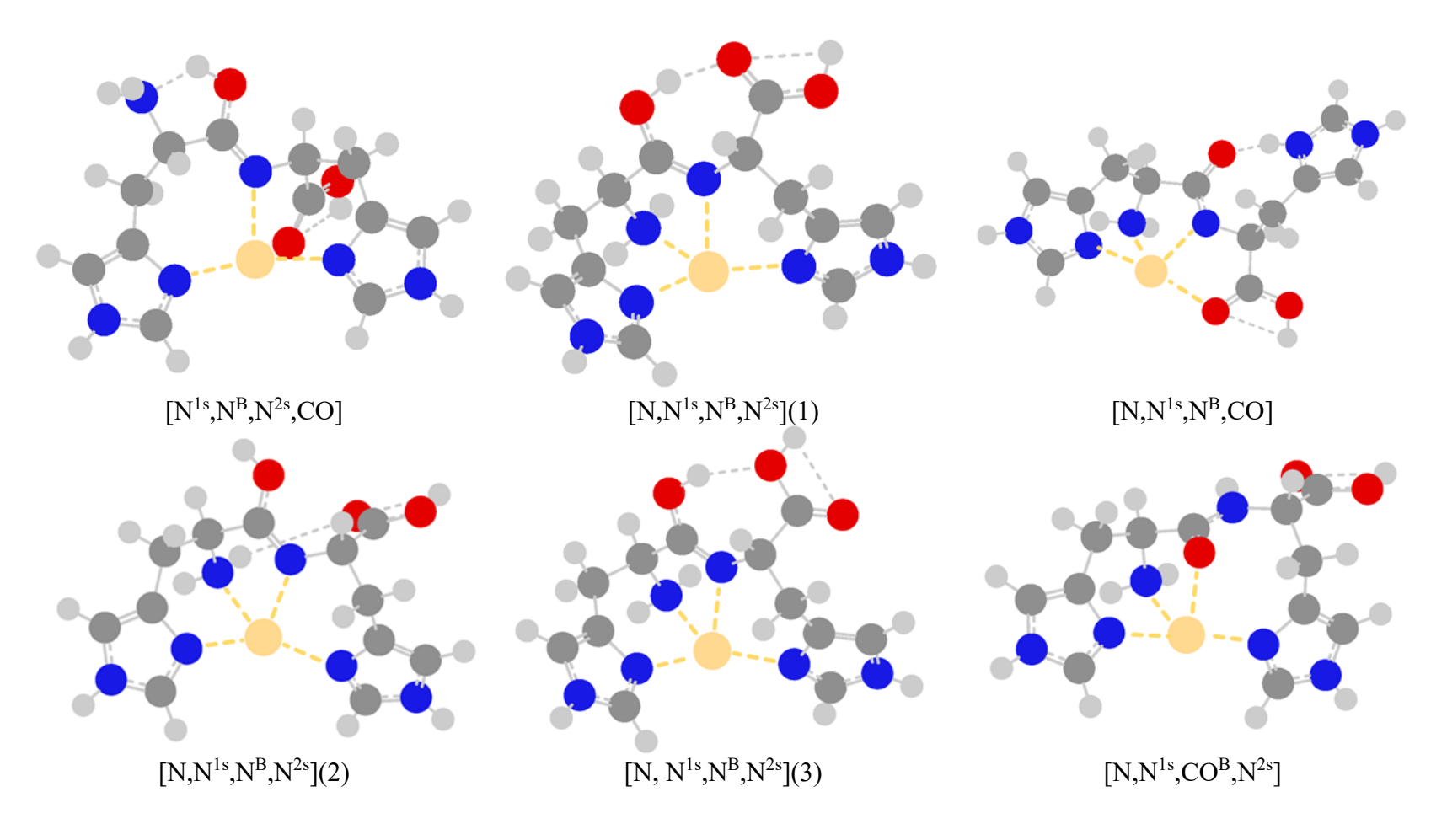


**Figure 3.** Structures of select Cd<sup>2+</sup>(HisHis) conformers calculated at the B3LYP/def2-TZVP level of theory. Red—oxygen, grey—carbon, white—hydrogen, blue—nitrogen, yellow—cadmium. Yellow dashed lines represent metal – ligand bonds.

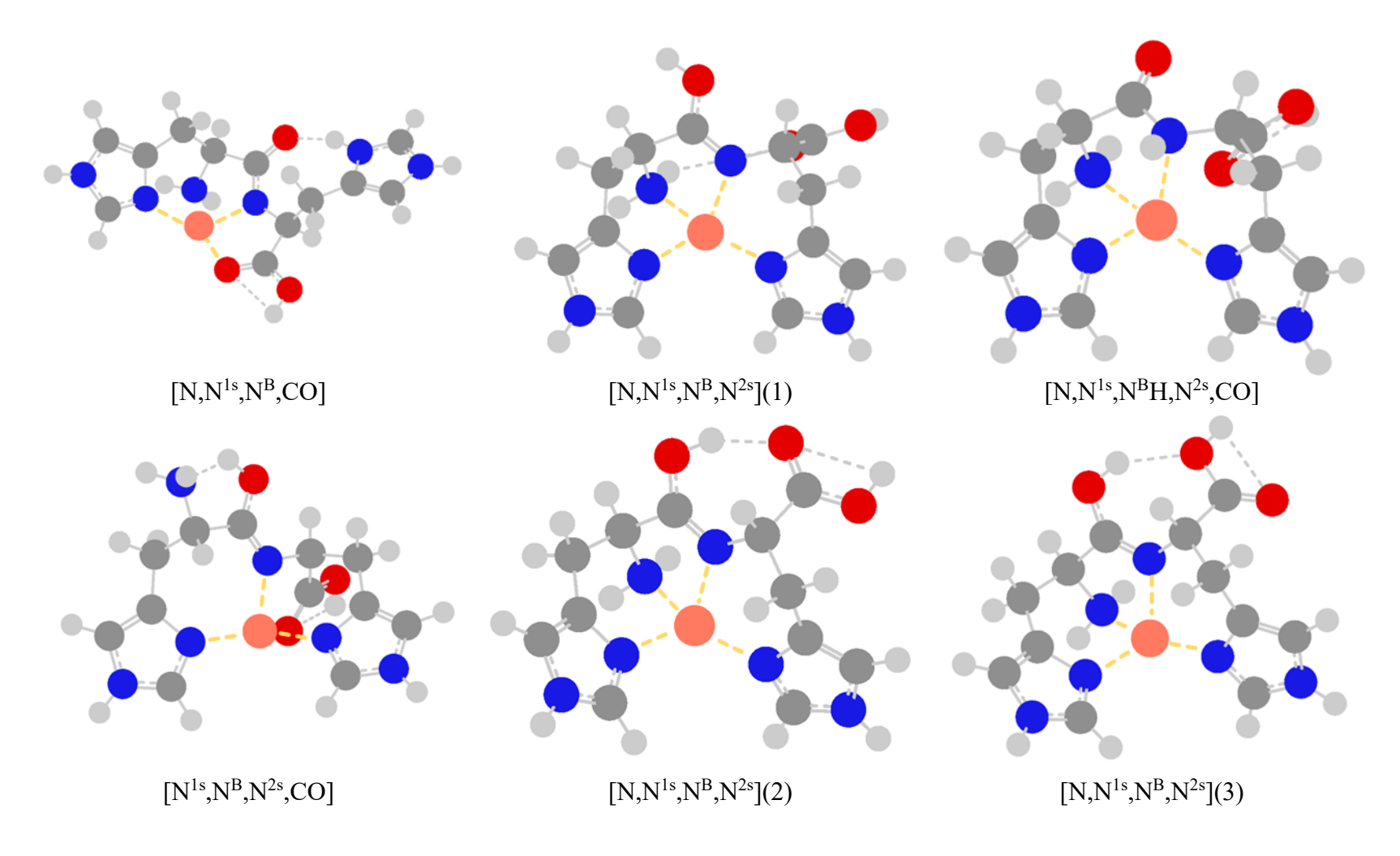


**Figure 4.** Structures of select Cu<sup>2+</sup>(HisHis) conformers calculated at the B3LYP/6-311+G(d,p) level of theory. Red—oxygen, grey—carbon, white—hydrogen, blue—nitrogen, orange—copper. Yellow dashed lines represent metal – ligand bonds.

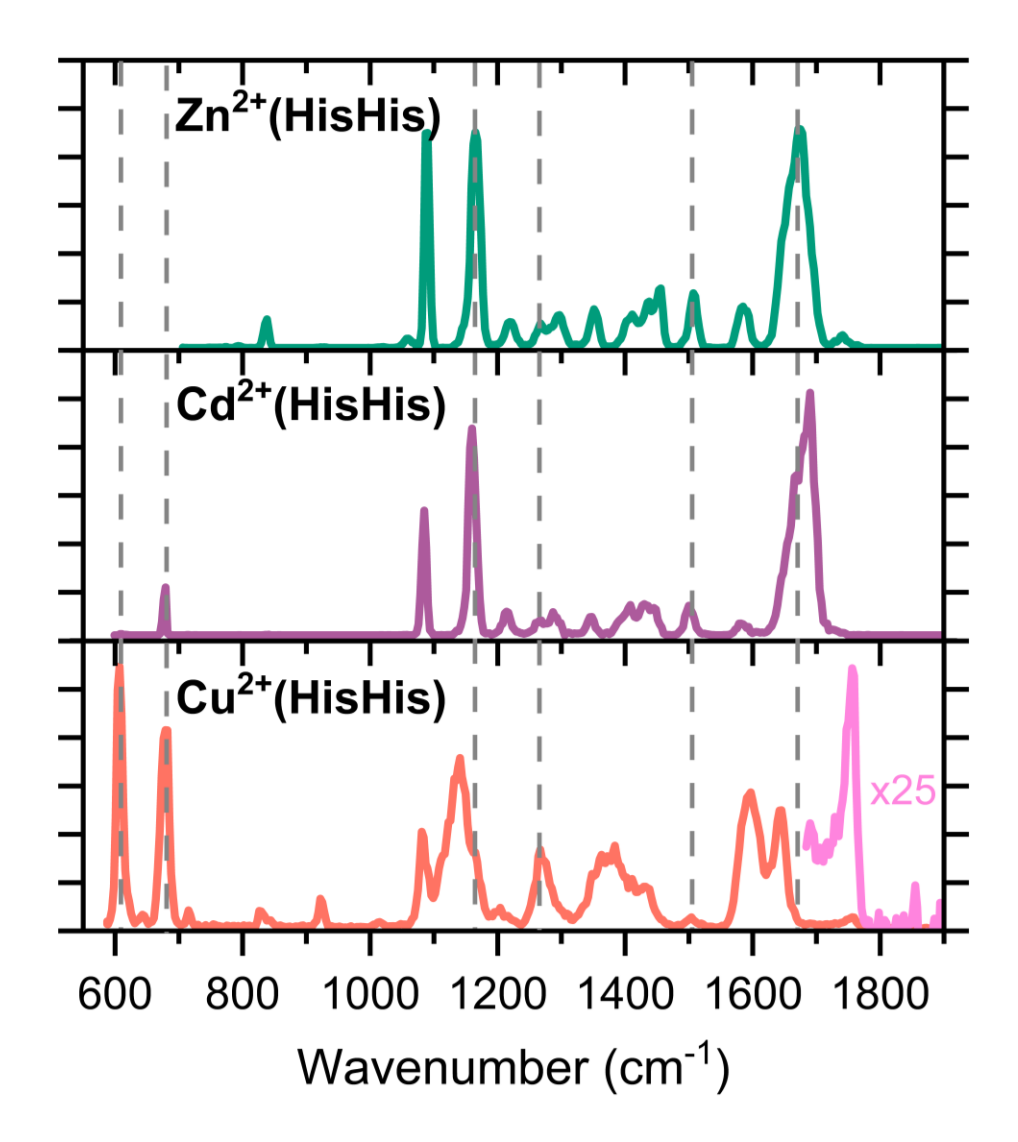


**Figure 5.** Comparison of the  $M^{2+}(HisHis)$  experimental IRMPD action spectrum. Grey dashed lines are placed to guide the eye. The inset in the bottom panel shows the  $Cu^{2+}(HisHis)$  spectrum between 1900 - 1700 cm<sup>-1</sup> magnified 25 times.

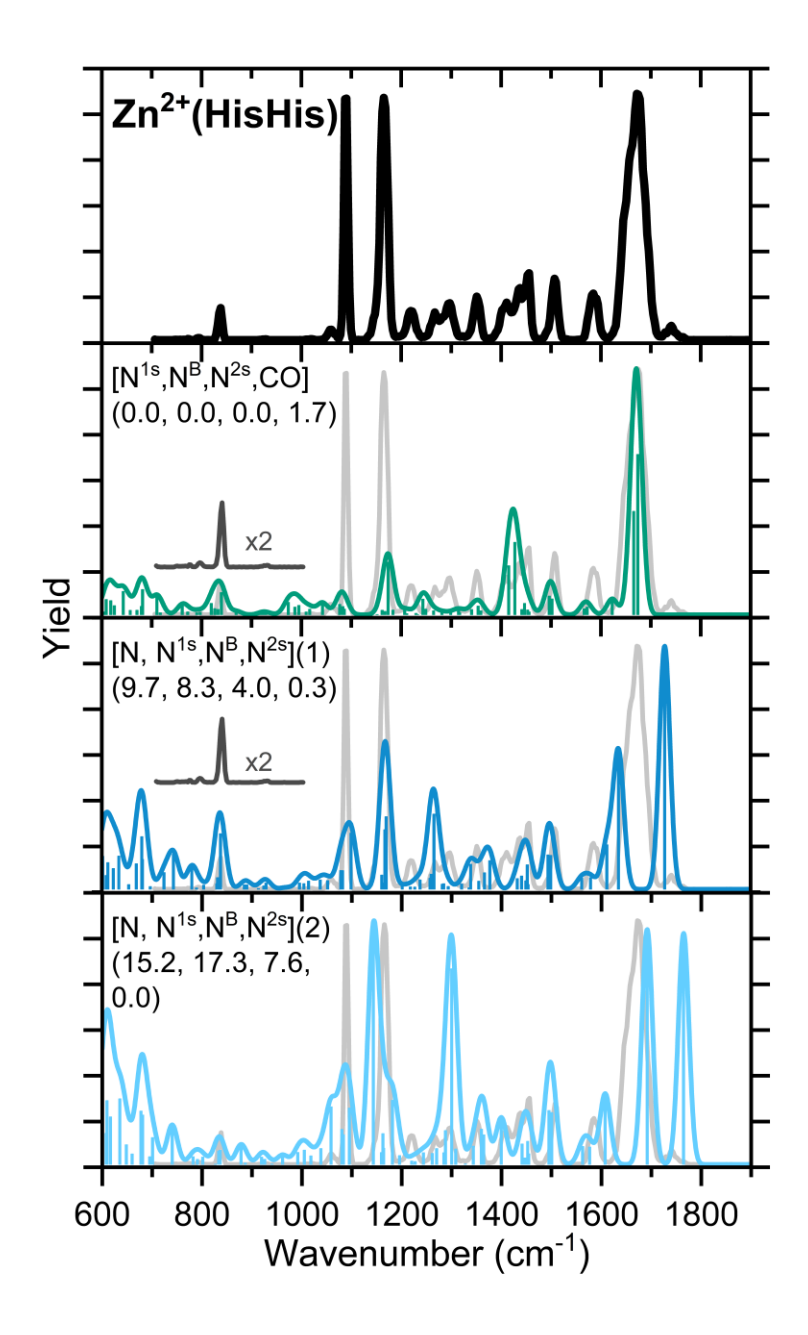


**Figure 6.** Comparison of the Zn<sup>2+</sup>(HisHis) experimental IRMPD action spectrum, shown here as the black line in the top panel and the light grey line in the three remaining panels, with IR spectra calculated at the B3LYP/6-311+G(d,p) level of theory for low-lying conformers. Relative 298 K Gibbs energies (kJ/mol) are listed at the B3LYP, B3P86, B3LYP-GD3BJ, and MP2 levels, respectively. The insets in the middle two panels show the Zn<sup>2+</sup>(HisHis) experimental spectrum magnified 2 times (dark grey line).

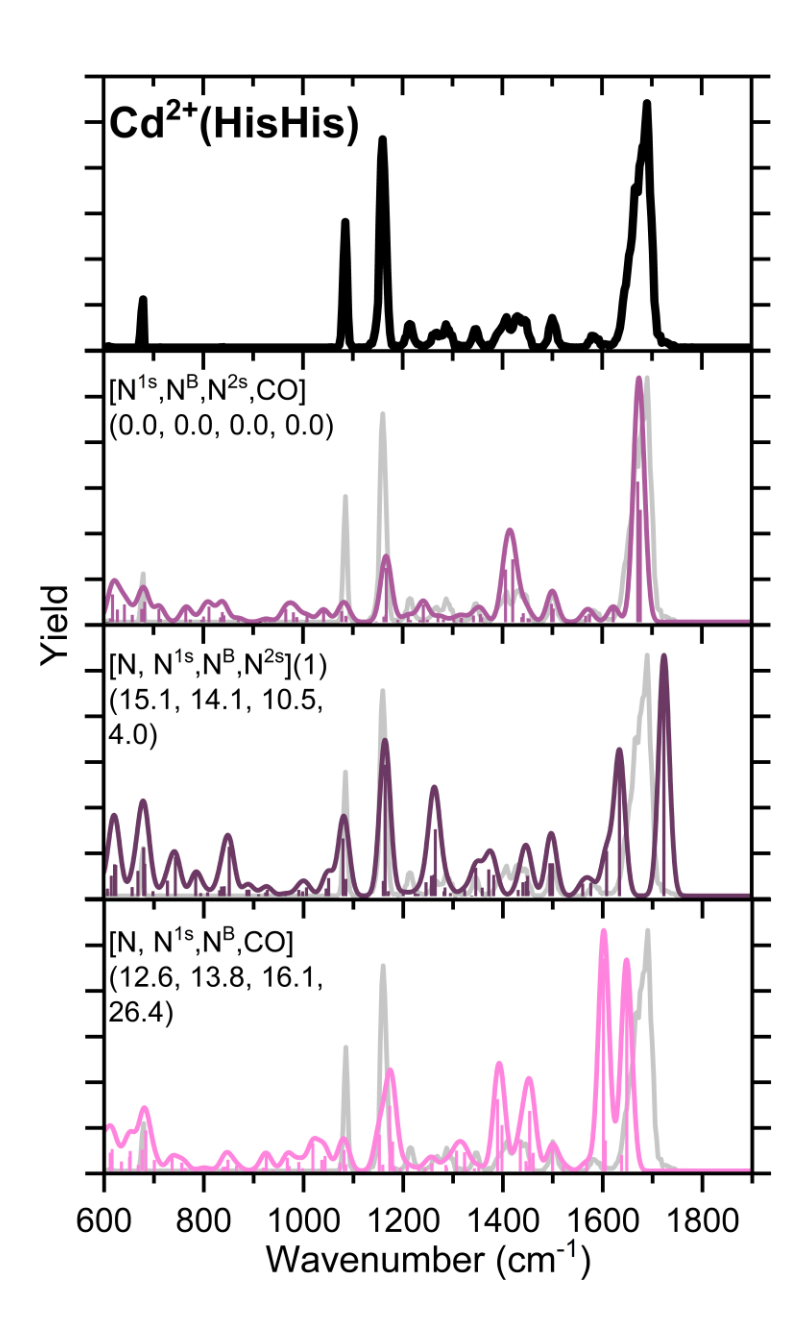


**Figure 7.** Comparison of the Cd<sup>2+</sup>(HisHis) experimental IRMPD action spectrum, shown here as the black line in the top panel and the light grey line in the three remaining panels, with IR spectra calculated at the B3LYP/def2-TZVP level of theory for low-lying conformers. Relative 298 K Gibbs energies (kJ/mol) are listed at the B3LYP, B3P86, B3LYP-GD3BJ, and MP2 levels, respectively.

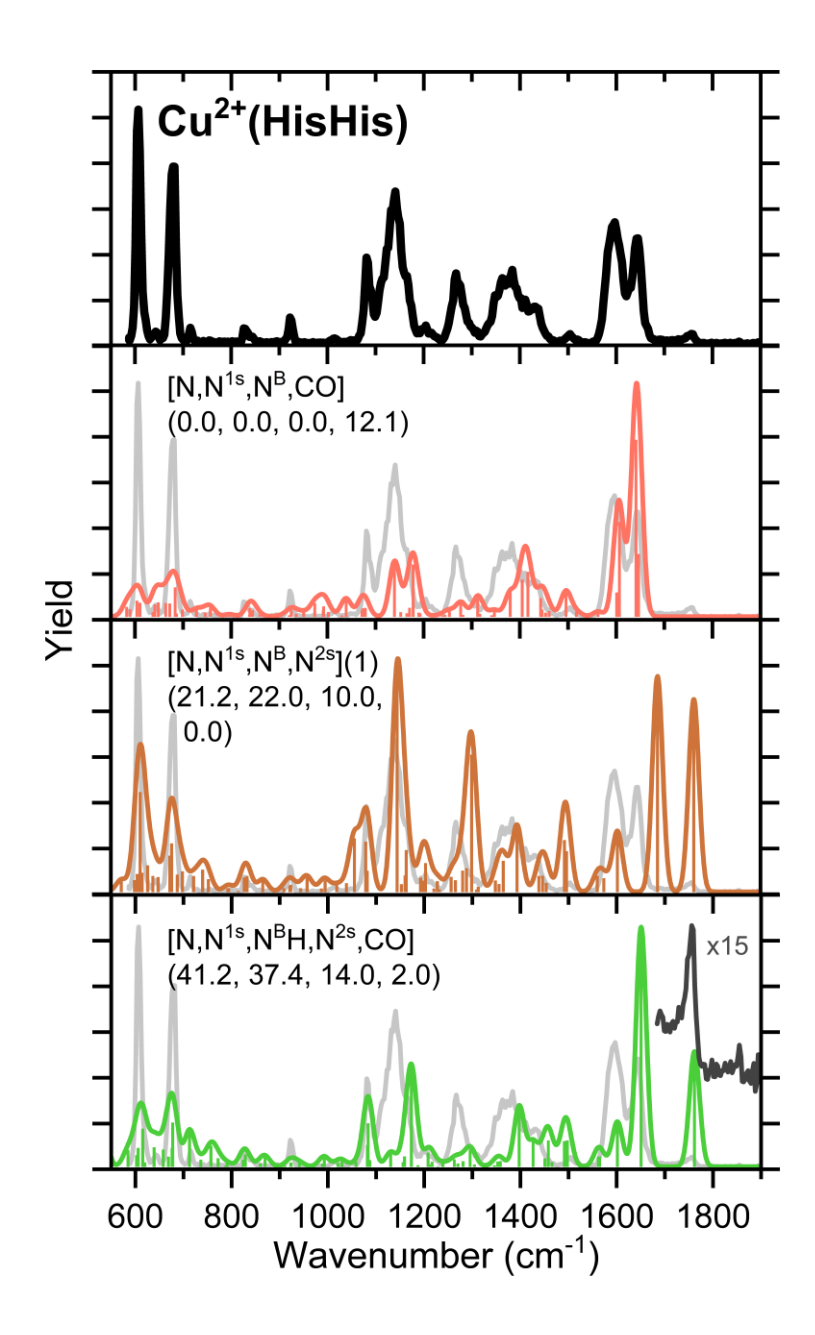


**Figure 8.** Comparison of the Cu<sup>2+</sup>(HisHis) experimental IRMPD action spectrum, shown here as the black line in the top panel and the light grey line in the three remaining panels, with IR spectra calculated at the B3LYP/6-311+G(d,p) level of theory for low-lying conformers. Relative 298 K Gibbs energies (kJ/mol) are listed at the B3LYP, B3P86, B3LYP-GD3BJ, and MP2 levels, respectively. The inset in the bottom panel shows the Cu<sup>2+</sup>(HisHis) experimental spectrum magnified 15 times (dark grey line).